Ocean Dynamics
DOI 10.1007/s10236-014-0713-x

Evaluation of nearshore wave models in steep reef environments

Mark Buckley · Ryan Lowe · Jeff Hansen

Received: 31 October 2013 / Accepted: 10 March 2014

Abstract To provide coastal engineers and scientists with a quantitative evaluation of nearshore numerical wave models in reef environments, we review and compare three commonly used models with detailed laboratory observations. These models are the following: (1) SWASH (Simulating WAves till SHore) (Zijlema et al. 2011), a phase-resolving nonlinear shallow-water wave model with added nonhydrostatic terms; (2) SWAN (Simulating WAve Nearshore) (Booij et al. 1999), a phase-averaged spectral wave model; and (3) XBeach (Roelvink et al. 2009), a coupled phase-averaged spectral wave model (applied to modeling sea-swell waves) and a nonlinear shallow-water model (applied to modeling infragravity waves). A quantitative assessment was made of each model's ability to predict sea-swell (SS) wave height, infragravity (IG) wave height, wave spectra, and wave setup ($\overline{\eta}$) at five locations across the laboratory fringing reef profile of Demirbilek et al. (2007). Simulations were performed with the "recommended" empirical coefficients as documented for each model, and then the key wave-breaking parameter for each model (α in SWASH and γ in both SWAN and XBeach) was optimized to most accurately reproduce the observations. SWASH, SWAN, and XBeach were found to be capable of predicting SS wave height variations across the steep fringing reef profile with reasonable accuracy using the default coefficients. Nevertheless, tuning of the key wave-breaking parameter improved the accuracy of each model's predictions. SWASH and XBeach were also able to predict IG wave height and spectral transformation. Although SWAN was capable of modeling the SS wave height, in its current form, it was not capable of modeling the spectral transformation into lower frequencies, as evident in the underprediction of the low-frequency waves.

Keywords Wave-breaking · Coral reefs · Breaking parameter · Nonlinear waves · Steep slope · Wave model · Wave dissipation

Responsible Editor: Rodrigo Cienfuegos

This article is part of the Topical Collection on the *7th International Conference on Coastal Dynamics in Arcachon, France 24-28 June 2013*

M. Buckley · R. Lowe · J. Hansen
School of Earth and Environment, University of Western Australia, Crawley, WA 6009, Australia

M. Buckley (✉) · R. Lowe · J. Hansen
The Oceans Institute, University of Western Australia, Crawley, WA 6009, Australia
e-mail: mark.buckley@uwa.edu.au

1 Introduction

Historically, nearly all nearshore wave models have primarily (or exclusively) been developed, calibrated, and tested on mild-slope sandy beaches. As a result, it is unclear if these models are suitable to simulate waves in reef systems that often have steep, sometimes nearly vertical, slopes and complex morphology. Here, we review three commonly used numerical nearshore wave models and quantitatively compare the model predictions with data from a detailed laboratory experiment of wave transformation across a model fringing reef. This evaluation provides insight into the suitability of each model to simulate a full range of hydrodynamic processes (sea-swell, infragravity waves, and wave setup) within reef systems as well as an assessment of where each model tends to break down and thus could be further improved.

Numerical wave models used to investigate field-scale processes on the order of kilometers to 10s of kilometers loosely fall into two categories: phase-averaged and phase-resolving (Cavaleri et al. 2007). Phase-averaged models simulate wave processes in a stochastic manner, often based on linear wave theory with empirical formulations derived from field or laboratory data. Phase-resolving models simulate wave processes

Published online: 10 May 2014

based on conservation laws (mass and momentum), but may also include empirical formulations calibrated to field or laboratory data. Phase-resolving models resolve individual waveforms, requiring a grid resolution fine enough to capture the shortest wave length (highest frequency waves) of interest in a study. This further increases the computational demand of such simulations, as the maximum allowable computational time step (dictated by the Courant condition) required to resolve wave propagation is dependent on the horizontal grid resolution and depth. Due to this computational demand, the application of phase-resolving wave models has been largely restricted to studies of lower frequency motions (e.g., infragravity waves, tsunamis, and tides), small-scale studies (e.g., a harbor entrance) and/or short duration dynamics, or idealized one-dimensional (1D) studies. Phase-averaged models, on the other hand, do not have the same restriction on grid resolution or time steps, allowing much larger scale and longer duration studies to be conducted. For larger scale and/or longer duration studies, which require modeling physical processes at a range of timescales (e.g., wind-waves, tides, and currents), both phase-resolving and phase-averaged models are often coupled.

The underlying assumptions embedded in existing nearshore wave models, e.g., spectral models and Boussinesq-type, that were originally developed for mild-slope beach environments are often technically violated when applied to reef environments (Massel and Gourlay 2000; Sheremet et al. 2011; Demirbilek and Nwogu 2007). For example, the steep slopes of coral reefs may violate the mild-slope assumption found in many weakly dispersive models (Demirbilek and Nwogu 2007). Additionally, parameterizations of bed stress, wave-breaking, and other processes developed originally for sandy beach environments may not be applicable. Due to the rapid bathymetric changes on reef slopes, wave-breaking is particularly intense and occurs across a much narrower region than the broad surf zone typically found on dissipative beaches. Further, due to the increased roughness, rates of bottom friction dissipation have also been shown to be much greater than on sandy beaches (e.g., Lowe et al. (2005)).

Despite these theoretical limitations, models and parameterizations originally derived for mild sandy slopes have often been applied to steep-slope reef environments with little or no modification. Symonds et al. (1995) first formulated a 1D analytical model for wave-driven currents on reefs, based on a linearized set of momentum equations and radiation stress theory. Subsequent 1D analytical models have been formulated by Hearn (1999) and Gourlay and Colleter (2005). Sheremet et al. (2011) compared a 1D nonlinear phase-averaged model and a 1D phase-resolving numerical model to laboratory data. Demirbilek and Nwogu (2007) and others have applied 1D Boussinesq-type models to laboratory data. Zijlema (2012) and Torres-Freyermuth et al. (2012) applied a nonhydrostatic nonlinear shallow-water wave model to laboratory and field datasets. Phase-averaged spectral wave models have been applied in field studies by Lowe et al. (2009), Hoeke et al. (2011), and Storlazzi et al. (2011) and tested against both laboratory and field data by Filipot and Cheung (2012). Pomeroy et al. (2012) and Van Dongeren et al. (2013) applied a coupled wave action and nonlinear shallow-water (NLSW) model to investigate the field-scale dynamics of short- and long-period wave motions across a fringing reef.

In this present study, three widely used open-source nearshore wave models are reviewed, and their performance is quantitatively compared against a comprehensive laboratory data set of wave transformation across a steep fringing reef profile under a range of different conditions. A particular focus of the assessment is on the dynamics of wave-breaking in the surf zone region and how this also influences predictions of low-frequency wave motions and wave setup. Each model was applied to 29 laboratory test conditions of Demirbilek et al. (2007), which incorporated a wide range of incident spectral wave conditions and still-water levels. Models were assessed for their performance in predicting sea-swell (SS) wave heights, infragravity (IG) wave heights, wave spectra, and wave setup ($\overline{\eta}$, the mean deviation from still water) at five locations across the fringing reef profile.

2 Numerical wave models

We selected three common nearshore wave models (Table 1). They are all open source, widely used, and span a range of modeling approaches (both phase-averaged and phase-resolving), theoretical complexities, and computational expense. These include the following: (1) SWASH (Simulating WAves till SHore; Version 1.20 downloaded from http://swash.sourceforge.net) (Zijlema et al. 2011), a phase-resolving nonhydrostatic free surface model; (2) SWAN (Simulating WAve Nearshore; Version 40.91 downloaded from http://swanmodel.sourceforge.net) (Booij et al. 1999), a phase-averaged spectral wave model; and (3) XBeach (Version 19; downloaded from http://oss.deltares.nl/web/xbeach) (Roelvink et al. 2009), a nearshore wave and circulation model that combines phase-averaged and phase-resolving approaches. As detailed descriptions of these three models are already widely available in the literature, only a brief overview of each is included here.

SWASH solves the nonlinear shallow-water equations with added nonhydrostatic pressure (Zijlema et al. 2011). Though the model is 3D for reasons of exposition Smit et al. (2013)

Table 1 Open-source numerical wave models evaluated in this study

Model	Class	Breaking formulation	Reference
SWASH	NLSW+nonhydrostatic terms	Shock capturing	(Zijlema et al. 2011)
SWAN	Wave action balance	Parametric	(Booij et al. 1999)
XBeach	Wave action balance with phase-resolving IG	Parametric	(Roelvink et al. 2009)

describe the governing equations in the 2D vertical plane with Cartesian, cross-shore (x) and vertical (z), coordinates, and time (t), as,

$$\frac{\partial u}{\partial t}+\frac{\partial uu}{\partial x}+\frac{\partial wu}{\partial z}=-\frac{1}{\rho}\frac{\partial(p_h+p_{nh})}{\partial x}+\frac{\partial \tau_{xx}}{\partial x}+\frac{\partial \tau_{xz}}{\partial z} \quad (1)$$

$$\frac{\partial w}{\partial t}+\frac{\partial uw}{\partial x}+\frac{\partial ww}{\partial z}=-\frac{1}{\rho}\frac{\partial p_{nh}}{\partial z}+\frac{\partial \tau_{zz}}{\partial z}+\frac{\partial \tau_{zx}}{\partial x} \quad (2)$$

$$\frac{\partial u}{\partial x}+\frac{\partial w}{\partial z}=0 \quad (3)$$

where $u(x,z,t)$ and $w(x,z,t)$ are the horizontal and vertical velocities, respectively, ρ is water density, p_h and p_{nh} are the hydrostatic and nonhydrostatic pressures, respectively, and τ_{xx}, τ_{xz}, τ_{zz}, , and τ_{zx} are the turbulent stresses.

SWAN predicts the spectral evolution of wave action in space and time (Booij et al. 1999). Wave action is defined as $A=E/\sigma$, where E is wave variance spectrum that distributes wave-energy over frequencies (σ) and propagation directions (θ). The governing wave action equation is (Booij et al. 1999)

$$\frac{\partial A}{\partial t}+\frac{\partial c_x A}{\partial x}+\frac{\partial c_y A}{\partial y}+\frac{\partial c_\sigma A}{\partial \sigma}+\frac{\partial c_\theta A}{\partial \theta}=\frac{S_{\text{tot}}}{\sigma} \quad (4)$$

where, c_x, c_y, c_σ, and c_θ are the propagation velocities of wave-energy in spatial (x, y), frequency (σ), and directional (θ) space, respectively. S_{tot} can include dissipation terms, in particular due to depth-limited wave-breaking and bottom friction as well as growth and energy transfer terms.

XBeach models SS wave processes in a phase-averaged manner, solving the wave action equation similar to Eq. (4) (Roelvink et al. 2009). However, the wave action equation in XBeach is solved for a single representative SS wave frequency and is applied at the timescale of individual wave groups. Appling the wave action equation at the timescale of individual wave groups allows variation in SS wave height and total water depth on the timescale of individual wave groups. Infragravity (IG) wave motions and mean flows are instead modeled in a phase-resolving manner, solving the nonlinear shallow-water equations (i.e., Eqs. (1, 2, and 3) but in a depth-averaged, hydrostatic form) (Roelvink et al. 2009). This allows XBeach to treat SS wave processes in a phase-averaged manner and long-wave processes (e.g., IG waves and tides) in a phase-resolving manner. This reduces the computational demand compared to a full (all frequencies) phase-resolving model.

2.1 Wave-breaking

There is no analytical solution for wave-breaking. Commonly used depth-integrated numerical wave models do not describe overturning of the free surface and thus cannot fully reproduce wave-breaking processes (Cienfuegos et al. 2010). Phase-resolving models of the Boussinesq-type commonly include wave-breaking effects by adding an ad hoc dissipation term, sometimes including roller effects, to the momentum equations (e.g., Svendsen (1984), Schäffer et al. (1993), and Madsen et al. (1997)). This method is referred to as an eddy viscosity approach. Eddy viscosity formulations require scaling coefficients with no direct physical or measurable meaning (Cienfuegos et al. 2010). The nonlinear shallow-water equations can be formulated to satisfy exact conservation laws (mass and momentum) for nondispersive waves (Zijlema et al. 2011; Smit et al. 2013). Implementation of exact conservation laws and use of numerical shock-capturing schemes, which solve for discontinuous hydraulic problems, allow wave-breaking dissipation to be modeled in a manner similar to hydraulic jumps (Zijlema and Stelling 2008).

SWASH accounts for depth-limited wave-breaking with a shock-capturing conservation scheme (Zijlema and Stelling 2008). In SWASH, with a large number of vertical layers, as waves steepen and approach breaking, a sawtooth waveform develops. At this discontinuity, the correct amount of energy is dissipated numerically via a shock-capturing scheme (Zijlema et al. 2011). When using only a single vertical layer, the sawtooth waveform is unable to develop due to the lack of vertical resolution of flow velocity. This requires an additional metric to determine the onset of wave-breaking (i.e., Smit et al. (2013))

$$\frac{\partial \eta}{\partial t}>\alpha\sqrt{g\left(h+\overline{\eta}\right)} \quad (5)$$

where α is an empirical tuning parameter that determines the onset of the breaking process, g is acceleration due to gravity, $h+\overline{\eta}$ is the time-averaged total water depth, composed of the still-water depth h, and the mean free surface variation $\overline{\eta}$ also referred to as wave setup. When the condition in Eq. (5) is met, nonhydrostatic pressure terms are removed locally allowing for the development of a sawtooth waveform. The default value of α=0.6 corresponds to a local wave front slope of roughly 25°.

Phase-averaged models use empirical (parametric) formulations to predict the rate of wave-energy dissipation during the wave-breaking process. These formulations generally include a method for estimating a probability distribution for the fraction of waves that are breaking (Q_b) and apply an energy dissipation rate using a theory for idealized bores (D_b) (Apotsos et al. 2007). SWAN and XBeach both implement parametric wave-breaking formulations.

SWAN (by default) uses the Battjes and Janssen (1978) formulation (herein, after BJ78). BJ78 calculates the mean energy dissipation per unit horizontal area due to depth-limited wave-breaking, D_{tot}, as

$$D_{\mathrm{tot}} = D_b Q_b \tag{6}$$

where D_b is the energy dissipation rate of an idealized individual breaking wave and Q_b is the time-averaged fraction of breaking or broken waves. D_b is calculated as

$$D_b = \frac{1}{4}\rho g f_{\mathrm{mean}} B H_{\mathrm{max}}^2 \tag{7}$$

where f_{mean} is the mean wave frequency, B is an empirical breaking intensity coefficient (by default B=1), and H_{max} is the maximum possible individual wave height in a total local water depth. H_{max} is calculated as

$$H_{\mathrm{max}} = \gamma(h+\overline{\eta}) \tag{8}$$

where γ is an empirical "breaker parameter." While γ is related to the maximum wave height to water depth ratio ($\gamma = H_{\mathrm{max}}/(h+\overline{\eta})$), in practice, it is usually used as a model tuning parameter.

Q_b varies between 0 to 1, with 0 representing no breaking and 1 representing complete breaking. In BJ78, Q_b is estimated from a Rayleigh wave-height distribution truncated at H_{max}.

$$\frac{1-Q_b}{\ln Q_b} = -8\frac{E_{\mathrm{tot}}}{H_{\mathrm{max}}^2} \tag{9}$$

where E_{tot} is the total wave-energy variance.

XBeach (by default) uses a modified form of the parametric dissipation formulation of Roelvink (1993) (hereafter R93). D_{tot} is calculated in the same manner as in Eq. (6) but with D_b calculated as

$$D_b = \frac{1}{4}\rho g f_{\mathrm{rep}} B H_{\mathrm{rms,SS}}^2 \frac{H_{\mathrm{rms,SS}}}{h+\overline{\eta}'} \tag{10}$$

where f_{rep} is a representative frequency, B is the breaking intensity coefficient (by default B=1), $H_{\mathrm{rms,SS}}$ is the root mean square (rms) wave height in the SS frequency band, and $\overline{\eta}'$ is the water-level deviation from h on the timescale of individual wave groups. The fraction of breaking waves is calculated as (Roelvink 1993)

$$Q_b = 1-\exp\left[-\left(\frac{H_{\mathrm{rms,SS}}}{H_{\mathrm{max}}}\right)^n\right], H_{\mathrm{max}} = \frac{\gamma \tanh k\left(h+\overline{\eta}'\right)}{k} \tag{11}$$

where n is a coefficient (n=10 by default; see Roelvink (1993) for discussion) and k is the wave number. There are thus several key differences between BJ78 and R93, as they are implemented in SWAN and XBeach, respectively. The BJ78 D_b formulation is dependent on wave frequency and water depth, whereas the R93 D_b formulation is dependent on wave frequency as well as the local values of $H_{\mathrm{rms,SS}}^2$ and $H_{\mathrm{rms,SS}}/(h+\overline{\eta}')$. Also, in XBeach, due to the separation of SS and IG waves, D_{tot} is applied only to SS waves; however, in SWAN, D_{tot} is applied to the entire wave spectrum and distributed at a rate proportional to the wave-energy variance at each frequency.

2.2 Bottom stress

Wave-energy and momentum are dissipated due to bottom stresses, which are related to the turbulent vertical fluxes of horizontal momentum (Feddersen et al. 2003). Wave and current bottom stresses are commonly treated independently using quadratic bottom friction formulations with an empirical friction coefficient. SWAN and XBeach each include a term for SS wave-energy dissipation due to bottom roughness in the wave action equation. SWASH and XBeach both add terms to the momentum equations to account for dissipation due to bottom roughness. Although bottom stress is known to be an important source of wave dissipation in coral reef environments (e.g., Lowe et al. (2005)), in this paper, we chose to focus mainly on wave-breaking dissipation.

3 Model application to a laboratory reef

Laboratory experiments by Demirbilek et al. (2007) were used to assess the performance of each of the numerical models. The laboratory study, conducted in a wind-wave flume at the University of Michigan, consisted of 29 test conditions carried

out on a 1:64 scale model of a fringing reef type profile typical of the southeast coast of Guam (Fig. 1). The flume was 35-m long, 0.7-m wide, and 1.6-m high, with smooth side walls and a smooth plastic bed. With the geometric scaling factor of 1:64, the flume length corresponds to a transect length of 2.24 km in the field. The fringing reef profile consisted of a composite slope with a 1:10.6 fore reef slope, a 4.8-m (~300-m field scale) long horizontal reef flat, and a 1:12 sloping beach (Fig. 1). The duration of simulations was 900 s (2-h field scale with 1:8 Froude scaling of time) with the final 800 s used in the analysis. Water-surface elevations were measured using eight capacitance type wave gauges with a sampling frequency of 20 Hz (2.5-Hz field scale). Irregular waves based on a JONSWAP (Hasselmann et al. 1980) spectrum (peak enhancement factor 3.3) were generated with a wedge-type wave maker with significant wave heights up to 10 cm (6.4-m field scale) and peak periods from 1.0 to 2.5 s (8- to 20-s field scale). The still-water depth over the reef flat (h_r) was also varied. A summary of the conditions during the 29 test conditions are included in Table 2.

Simulations were initially performed using "recommended" model coefficient values (hereafter, referred to as "untuned" simulations) as documented for each model. This provides an estimate of the errors expected in the application of an untuned model. Testing the untuned models is crucial as in many cases, limited or no calibration data is available and in practice, untuned models are frequently relied upon to provide predictive skill. This testing is particularly important in enviroments such as reefs, which differ from the traditional beach environments used to establish the "default" untuned wave-breaking parameters. The key depth-limited wave-breaking parameter for each model (α in SWASH and γ in both SWAN and XBeach) was then systematically varied over a full range of physically reasonable values in order to determine the optimal values for each test condition. Extensive testing of the key wave-breaking parameter within each model gives insight into each model's response to the free parameter allowing the sensitivity, tune-ability, and appropriate values to be assessed.

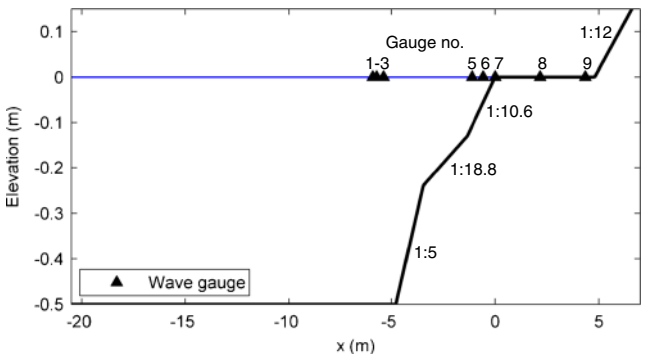

Fig. 1 Laboratory setup for the University of Michigan flume experiment (Demirbilek et al. 2007)

3.1 Model setup

Numerical simulations were performed with each model configured in a 1D mode using a uniform horizontal grid size of 0.02 m with a minimum threshold water depth of 0.005 m. SWASH and XBeach simulations were run for durations of 900 s, with a time step determined by imposing a maximum Courant number of 0.5. SWAN simulations were performed in a stationary mode. All models were forced on the offshore boundary with a wave-energy spectra derived for each test condition from the measured water-level time series at the offshore gauges (gauges 1–3; Fig. 1). Directional filtering of the offshore water level gauges was performed, using a three-point method (Mansard and Funke 1980), to remove offshore directed wave-energy. To simulate the smooth plastic bed of the flume, a dimensionless friction coefficient of c_f=0.001 was used for SWASH and XBeach simulations. This low c_f value had a negligible contribution to the overall wave dissipation, which was overwhelmingly dominated by wave-breaking. The wave action equations for SWAN and XBeach include an optional term parameterizing wave frictional dissipation; by default, this term is neglected in XBeach and included in SWAN. Here, we do not include SS wave friction in the simulations. This is also consistent with Filipot and Cheung (2012), who neglect wave friction when applying SWAN to the same dataset.

Following Zijlema (2012), SWASH was run with the discrete upwind momentum-conservative advection scheme. Although SWASH can be configured with multiple vertical layers, here, only a single vertical layer is implemented. Depth-limited wave-breaking was accounted for with the onset of breaking controlled by α=0.6 in the untuned case. α was varied from 0.1 to 5.0 in increments of 0.01 in the sensitivity analysis. Water-level time-series output from the model were then exported at the gauge locations at 20 Hz.

SWAN was run in a stationary mode with triad interactions and frequency shifts activated, wave setup activated, and white-capping deactivated. The simulations were performed with 36 directional bins from 0 to 360° and 42 logarithmically distributed frequency bins from 0.01 to 10 Hz. Depth-limited wave-breaking was modeled using the BJ78 formulation with the default γ=0.73 for the untuned case. However, γ was varied from 0.1 to 1.2 in increments of 0.01 in the sensitivity analysis. 1D wave-energy spectra were exported from SWAN at the gauge locations.

Depth-limited wave-breaking in XBeach was modeled using the R93 formulation with the default γ=0.55 for the untuned case. Like SWAN, γ was varied from 0.1 to 1.2 in increments of 0.01 for the sensitivity analysis. By default, XBeach includes a roller energy balance; this was activated in the current study with the default *beta* (roller face slope (Reniers and Battjes 1997)) value of 0.1. Water-level time series were exported at the gauge locations at 20 Hz.

Table 2 Summary of the 29 test conditions, tuned values of the key breaking parameter for SWASH, SWAN, and XBeach, and percent error reduction owing to model tuning (BSS)

					SWASH				SWAN				XBeach			
Test no.	$H_{rms,SS}$ (m)	T_p (s)	h_r (m)	F_{c0}	Tuned α	BSS SS (%)	BSS IG (%)	BSS $\overline{\eta}$ (%)	Tuned γ	BSS SS (%)	BSS IG (%)	BSS $\overline{\eta}$ (%)	Tuned γ	BSS SS (%)	BSS IG (%)	BSS $\overline{\eta}$ (%)
15	0.044	0.98	0.051	4.84E+02	0.60	0	0	0	0.70	81	13	21	0.36	85	−47	−8
16	0.037	1.42	0.051	1.23E+03	0.85	57	−35	−5	0.64	82	−2	92	0.33	91	57	19
17	0.055	1.42	0.051	1.36E+03	1.19	57	−22	3	0.65	43	−1	19	0.35	83	−26	−14
18	0.059	1.97	0.051	2.73E+03	1.15	74	50	−19	0.64	21	0	−105	0.34	83	20	−13
19	0.057	2.56	0.051	4.56E+03	1.90	77	31	−32	0.71	49	0	−27	0.33	76	42	−19
20	0.043	1.22	0.051	8.30E+02	0.90	67	33	−7	0.66	85	−3	92	0.35	89	−105	17
21	0.057	1.83	0.051	2.00E+03	1.09	83	−8	−9	0.73	0	0	0	0.33	85	28	−6
26	0.041	0.98	0.016	1.95E+03	0.61	11	44	−26	0.63	30	−1	−9	0.24	85	−206	−136
27	0.039	1.22	0.016	3.14E+03	0.80	16	−5	−5	0.68	10	0	−2	0.27	84	−159	−71
28	0.033	1.42	0.016	4.68E+03	1.00	1	3	8	0.68	81	−2	43	0.27	84	−15	−47
29	0.050	1.51	0.016	4.44E+03	0.70	14	−4	−6	0.70	65	−1	66	0.34	76	−208	−68
30	0.053	1.83	0.016	6.19E+03	0.20	28	6	−8	0.65	75	−1	82	0.29	81	61	−111
31	0.059	1.97	0.016	8.10E+03	0.18	35	0	48	0.72	13	0	−36	0.35	76	59	27
32	0.055	2.56	0.016	1.27E+04	2.18	60	23	−152	0.69	4	0	−141	0.30	68	72	46
33	0.040	0.98	0.000	1.09E+04	2.50	44	−16	3	0.92	78	1	51	0.35	80	−68	−43
34	0.031	1.42	0.000	1.77E+04	3.24	87	−249	16	0.79	65	1	18	0.34	88	44	−3
35	0.031	1.42	0.000	1.80E+04	3.21	91	−115	15	0.85	72	1	40	0.33	85	28	2
36	0.048	1.51	0.000	1.25E+04	3.46	83	66	−59	0.85	44	0	42	0.35	83	−118	−175
37	0.053	1.83	0.000	1.65E+04	2.69	53	6	−372	0.83	59	0	12	0.33	84	70	66
38	0.058	1.97	0.000	2.00E+04	0.39	38	6	21	0.71	10	0	−9	0.34	79	45	20
39	0.054	2.56	0.000	2.97E+04	3.11	57	−19	−112	0.45	27	0	−1,561	0.40	73	9	19
44	0.022	0.98	0.031	2.48E+02	0.65	1	4	−1	0.61	28	−2	2	0.30	72	−69	7
45	0.043	0.98	0.031	1.04E+03	1.15	18	5	−6	0.71	4	0	−12	0.34	75	−68	−9
46	0.041	1.22	0.031	1.70E+03	1.36	33	−27	−5	0.65	61	−3	92	0.34	79	−103	−13
47	0.035	1.42	0.031	2.53E+03	1.15	22	−27	0	0.66	58	−2	51	0.33	84	−3	5
48	0.052	1.42	0.031	2.62E+03	1.28	44	−34	−3	0.65	27	−2	63	0.36	76	−272	−44
57	0.054	1.83	0.031	3.62E+03	1.83	47	34	−20	0.75	15	0	3	0.35	85	0	−37
58	0.059	1.97	0.031	5.01E+03	1.50	50	5	−73	0.72	52	0	44	0.37	81	16	−28
59	0.057	2.56	0.031	8.12E+03	1.78	54	5	−20	0.72	18	0	7	0.35	74	61	−26

Negative values of BSS indicate a decrease in the accuracy of the tuned model predictions relative to the untuned model predictions

3.2 Data processing and performance metrics

Measured and simulated water-level time series were used to compute 1D wave-energy spectra $S(f)$ using Welch's averaged, modified periodogram method with a Hanning window and a segment length of 2^9 samples (~26 s). The SS rms wave height, $H_{rms,SS}$, was calculated as

$$H_{rms,ss} = \sqrt{8\int_{f_l}^{\infty} S\,df} \tag{12}$$

where f_l is the boundary between SS and IG frequency bands. In agreement with Sheremet et al. (2011) and others, f_l was taken as half the peak forcing frequency of each simulation (i.e., f_l=0.5f_p). XBeach uses a representative frequency for the SS band and does not model the SS spectra; thus, the mean $H_{rms,SS}$ for XBeach was exported directly from the model. Likewise, for IG rms wave height, $H_{rms,IG}$ was calculated as

$$H_{rms,IG} = \sqrt{8\int_{0}^{f_l} S\,df} \tag{13}$$

Following Apotsos et al. (2008), model performance was quantified using the weighted rms percent error metric (WRPE), defined as

$$\mathrm{WRPE} = \sqrt{\sum_n \left[\left(\frac{\mathrm{obs}_n - \mathrm{pred}_n}{\mathrm{obs}_n}\right)^2 \times \mathrm{weight}_n\right]} \times 100\% \tag{14}$$

$$\text{weight}_n = \frac{\text{dist}_{n-1} + \text{dist}_{n+1}}{\text{dist}_{\text{tot}}} \quad (15)$$

where n is the gauge number, obs and pred are the observed and predicted values, respectively, dist is the distance between gauges, and dist_{tot} is the total distance between all gauges. WRPE was calculated for $H_{\text{rms,SS}}$, $H_{\text{rms,IG}}$, and $\overline{\eta}$, denoted WRPE SS, WRPE IG, and WRPE $\overline{\eta}$, respectively. Offshore gauges used for the model boundary forcing condition were excluded from this analysis, and hence, only gauges 5–9 (Fig. 1) were used in the calculation. Model tuning was assessed using WRPE SS rather than a combination of WRPE SS and WRPE IG, given that depth-limited wave-breaking occurs primarily in the SS frequency band through the surf zone and wave-breaking formulations have been developed primarily to predict SS decay in the surf zone. The percent error reduction that can be achieved with model tuning was also estimated using the Brier Skill Score (BSS) (Murphy and Epstein 1989; Ruessink et al. 2003; Apotsos et al. 2008).

$$\text{BSS} = \left[1 - \frac{\text{WRPE}_{\text{tuned}}}{\text{WRPE}_{\text{untuned}}}\right] \times 100\% \quad (16)$$

We define BSS SS, BSS IG, and BSS $\overline{\eta}$ as the BSS based on WRPE SS, WRPE IG, and WRPE $\overline{\eta}$, respectively.

4 Results

4.1 Test no. 35

The laboratory observations showed a rapid dissipation of SS energy near the reef crest, an increase in the proportion of IG energy over the reef flat, and wave setup across the reef. Figure 2 shows an example of this observed wave transformation for test no. 35 ($H_{\text{rms,SS}}$=0.032 m (2.0-m field scale); T_p=1.42 (11-s field scale); h_r=0.00 m (0.0-m field scale)), which had an intermediate wave height and period. Test no. 35 also had its still-water level located at the elevation of the reef flat, which should provide a challenge for the models. Test no. 35 is used throughout this paper to highlight many of the common features of the broader set of test conditions. Wave-breaking near the reef crest resulted in the largest dissipation of SS and IG energy between gauges 6 (x=−0.57 m) and 7 (x=0.010 m) (Fig. 2). Offshore of the reef crest (x<0 m), the majority of the incident wave-energy is in the SS frequencies as expected (Fig. 2a). Between gauges 6 and 7, the majority of wave-breaking occurs with the strong dissipation of SS energy resulting in an increasing proportion of IG energy. The proportion of IG to SS energy further increases on the reef flat, with $H_{\text{rms,SS}}$ and $H_{\text{rms,IG}}$ becoming roughly equal magnitude over most of the reef flat (Fig. 2a, b).

With untuned wave-breaking parameters, SWASH (α=0.6) and SWAN (γ=0.73) reproduced observed SS wave transformation well (Fig. 3a). XBeach (γ=0.55) slightly overpredicted $H_{\text{rms,SS}}$ on the reef flat (Fig. 3a). For this test no. 35, tuning γ for XBeach gave a smaller than default optimal γ value of 0.33 (untuned γ=0.55), which corrected the overprediction of $H_{\text{rms,SS}}$ on the reef flat and reduced the WRPE SS by 85 % (Fig. 3a, e; Table 2). This tuning of XBeach, however, resulted in an underestimate of $H_{\text{rms,SS}}$ at gauges 5 and 6 (Fig. 3e). Conversely, tuning SWAN gave a greater than default optimal γ value of 0.85 (untuned γ=0.73) with a WRPE SS reduction of 72 % (Table 2). Tuning SWASH gave a much greater optimal α value of 3.21 compared to the untuned value of α=0.6, with a WRPE SS reduction of 91 % (Table 2).

For test no. 35 ($H_{\text{rms,SS}}$=0.032 m; T_p=1.42; h_r=0.00 m), model performance in predicting the IG wave transformation was more varied (Fig. 3b, f). SWASH and XBeach reproduced the overall IG development across the reef relatively well using the untuned breaking parameters; however, SWAN greatly underpredicted IG energy across the reef profile and showed nearly complete dissipation of IG energy on the reef flat (Fig. 3b, f).

When the key wave-breaking parameters were tuned to minimize WRPE SS, this had varying effects on the accuracy of the IG prediction in both models (Table 2 BSS IG). For SWASH, tuning α to optimize the $H_{\text{rms,SS}}$ prediction resulted in a drastic decrease in the accuracy of the IG wave predictions (BSS IG=−115 %; Table 2). Conversely, for XBeach, tuning γ reduced the overprediction of $H_{\text{rms,IG}}$ on top of the reef and (BSS IG=28 %; Table 2). SWAN showed negligible improvement in the $H_{\text{rms,IG}}$ prediction with tuning (BSS IG=1 %; Table 2).

Wave setup $\overline{\eta}$ over the reef profile was well predicted with SWASH and XBeach for test no. 35 using the untuned breaking parameters, but was underpredicted using SWAN (Fig. 3c). These predictions were slightly improved when tuning the breaking parameters (Fig. 3g; Table 2).

Measured and predicted wave spectra are shown for test no. 35 for two sites: the shoaling region (gauge 6; Fig. 4a, c) and on the reef flat (gauge 8; Fig. 4b, d). At gauge 6, the majority of the energy was in the SS band, centered on the peak forcing frequency (indicated by the vertical black line; Fig. 4a, c). Measured wave-energy in the IG band was relatively constant between these two gauges. Directional (i.e., shoreward versus seaward) analysis of the offshore water level showed that a significant proportion of IG energy was propagating offshore. SWASH and SWAN accurately predicted the distribution of SS energy in the shoaling region (gauge 6; Fig. 4a, c) and the dissipation of SS energy on the reef flat (gauge 8; Fig. 4b, d). Note that XBeach simulates SS using a single representative frequency, so it is only possible to compare the low-frequency spectra for XBeach.

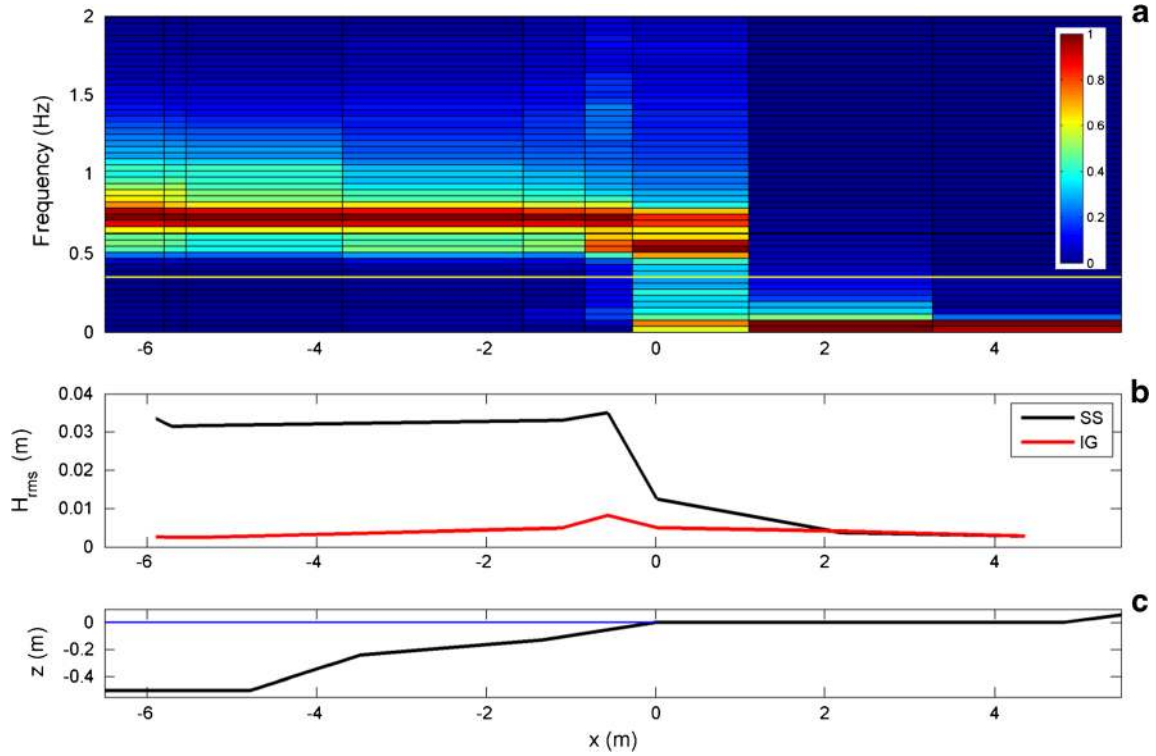

Fig. 2 Measured wave parameters for test no. 35 ($H_{rms,SS}$=0.032 m; T_p=1.42; h_r=0.00 m). **a** Normalized wave-energy spectrum (normalized by maximum spectral density at a given location) at each gauge locations. The *horizontal yellow line* gives the separation frequency between SS and IG. **b** $H_{rms,SS}$ and $H_{rms,IG}$. **c** Reef elevation profile

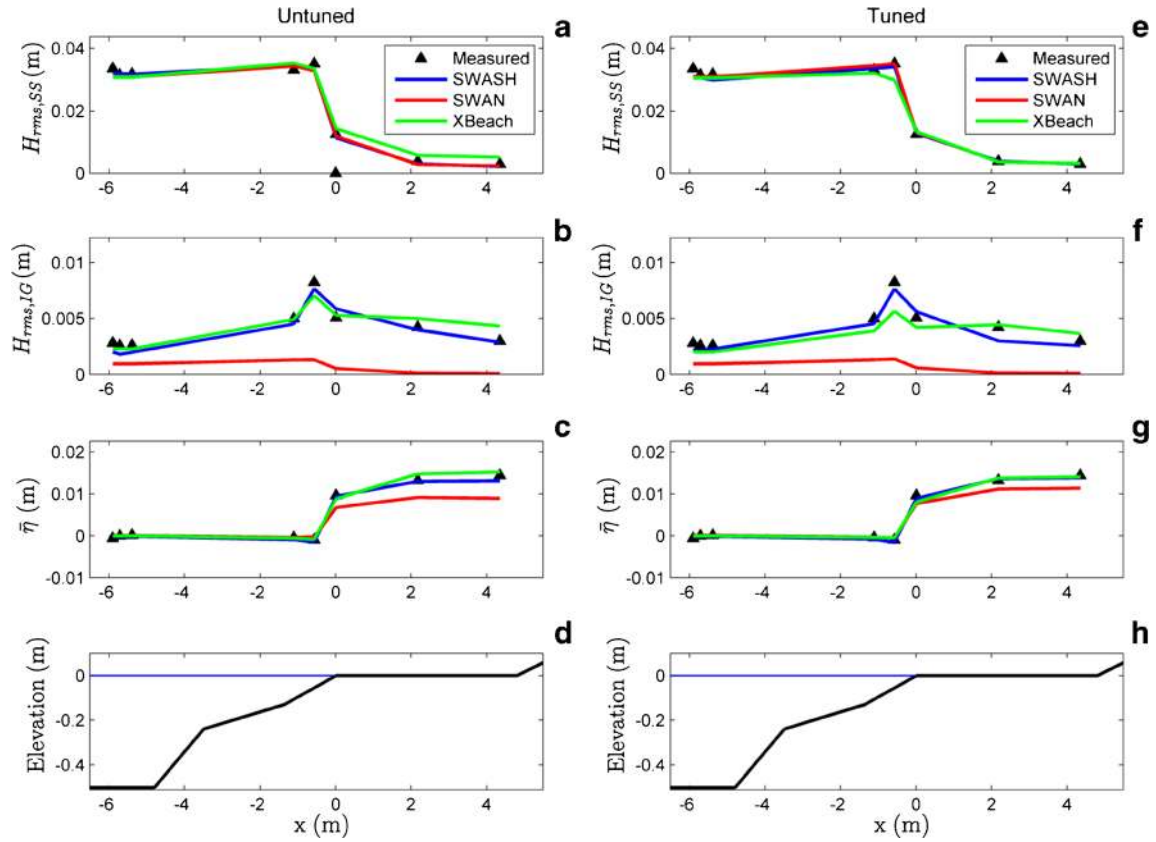

Fig. 3 **a**–**h** Measured and simulated $H_{rms,SS}$, $H_{rms,IG}$, and $\overline{\eta}$ across the fringing reef profile for test no. 35 ($H_{rms,SS}$=0.032 m; T_p=1.42; h_r=0.00 m). Model results for untuned (*left column*) and tuned (*right column*) breaking parameters. The reef elevation profile is shown (*bottom row*) for reference

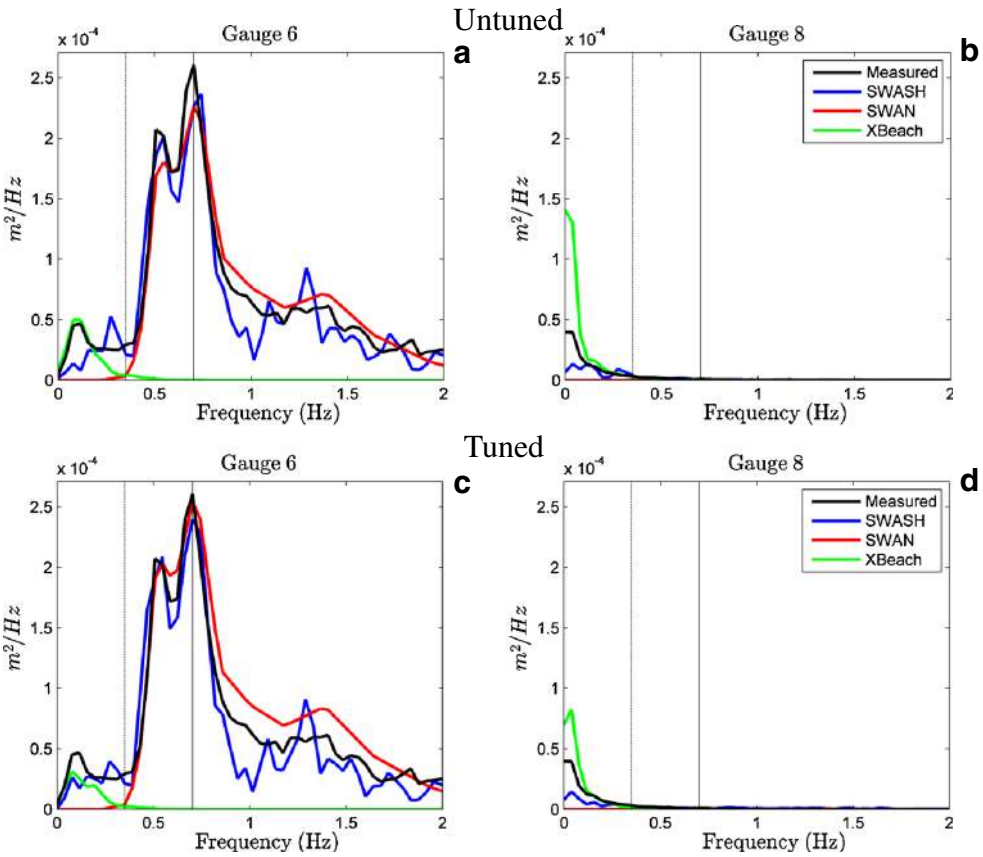

Fig. 4 Measured and simulated wave-energy spectra at **a**, **c** gauge 6 (shoaling region; *left column*) and **b**, **d** gauge 8 (reef flat; *right column*) for test no. 35 ($H_{rms,SS}$= 0.032 m; T_p=1.42; h_r=0.00 m). Model results for untuned (*upper row*) and tuned (*lower row*) breaking parameters are shown for SWASH (*blue line*), SWAN (*red line*), and XBeach (*green line*). The peak forcing frequency (*vertical solid black line*) and the SS-IG frequency cutoff (*vertical dashed black line*) are shown for reference. XBeach simulates SS waves using a single representative frequency, so it is only possible to compare the low-frequency spectra

4.2 Summary of all test conditions

When evaluating all test cases, SWASH and XBeach with untuned breaking parameters provided reasonable agreement with the measured wave heights (both $H_{rms,SS}$ and $H_{rms,IG}$) and $\overline{\eta}$ for all 29 conditions (Fig. 5). SWAN accurately predicted $H_{rms,SS}$, but failed to predict $H_{rms,IG}$ (Fig. 5, middle row). Predicted $\overline{\eta}$ for SWAN showed considerably more error than SWASH and XBeach (Fig. 5, bottom row). For all three models, the accuracy of $H_{rms,SS}$ predictions were improved by tuning the wave-breaking parameters (Table 2; Fig. 6). The maximum WRPE SS for all of the untuned models and all test cases was 92 %, but with tuning, the maximum WRPE SS was reduced to <17 % (Table 2; Fig. 7). Predictions of $H_{rms,SS}$ were improved most notably with tuning for XBeach (Fig. 7). Tuning the breaking parameters to minimize WRPE SS gave mixed results in terms of the accuracy of both the $H_{rms,IG}$ and $\overline{\eta}$ predictions with some tests showing an improvement and others showing a substantial decrease in accuracy (Fig. 7).

5 Discussion

The key wave-breaking parameters in SWASH (α), SWAN (γ), and XBeach (γ) have some physical basis, but in practice are mainly used as free parameters utilized to calibrate wave models.

5.1 The role of α in SWASH

The α breaking parameter within the shock-capturing scheme in SWASH controls the onset of breaking when the criteria given by Eq. (5) $\partial\eta/\partial t > \alpha\sqrt{g(h+\overline{\eta})}$ is satisfied. Given that $\partial\eta/\partial t$ is kinematically related to the slope of the free surface $\partial\eta/\partial x$ for a progressive wave; higher values of α increase the threshold surface slope for the onset of wave-breaking, thus allowing for steeper wave faces prior to wave-breaking and moving the break point shoreward. In general, increasing α allows for a larger wave height to develop prior to breaking and in our case increases the maximum breaking dissipation (dissipation between gauges 6 and 7), but decreases the width of the surf zone thereby increasing $H_{rms,SS}/(h+\overline{\eta})$ on the reef flat. Optimal α values averaged 1.5, considerably higher than the untuned value of 0.6 (Table 2), implying that the wave face prior to breaking was steeper (~55°) than the default value of α=0.6 (~25°). This is physically consistent with the occurrence of plunging breakers on the steep fore reef slope, although no detailed data to confirm breaking wave slope (e.g., from video imagery) are available in the Demirbilek et al. (2007) study. But the laboratory study of Ting and Kirby

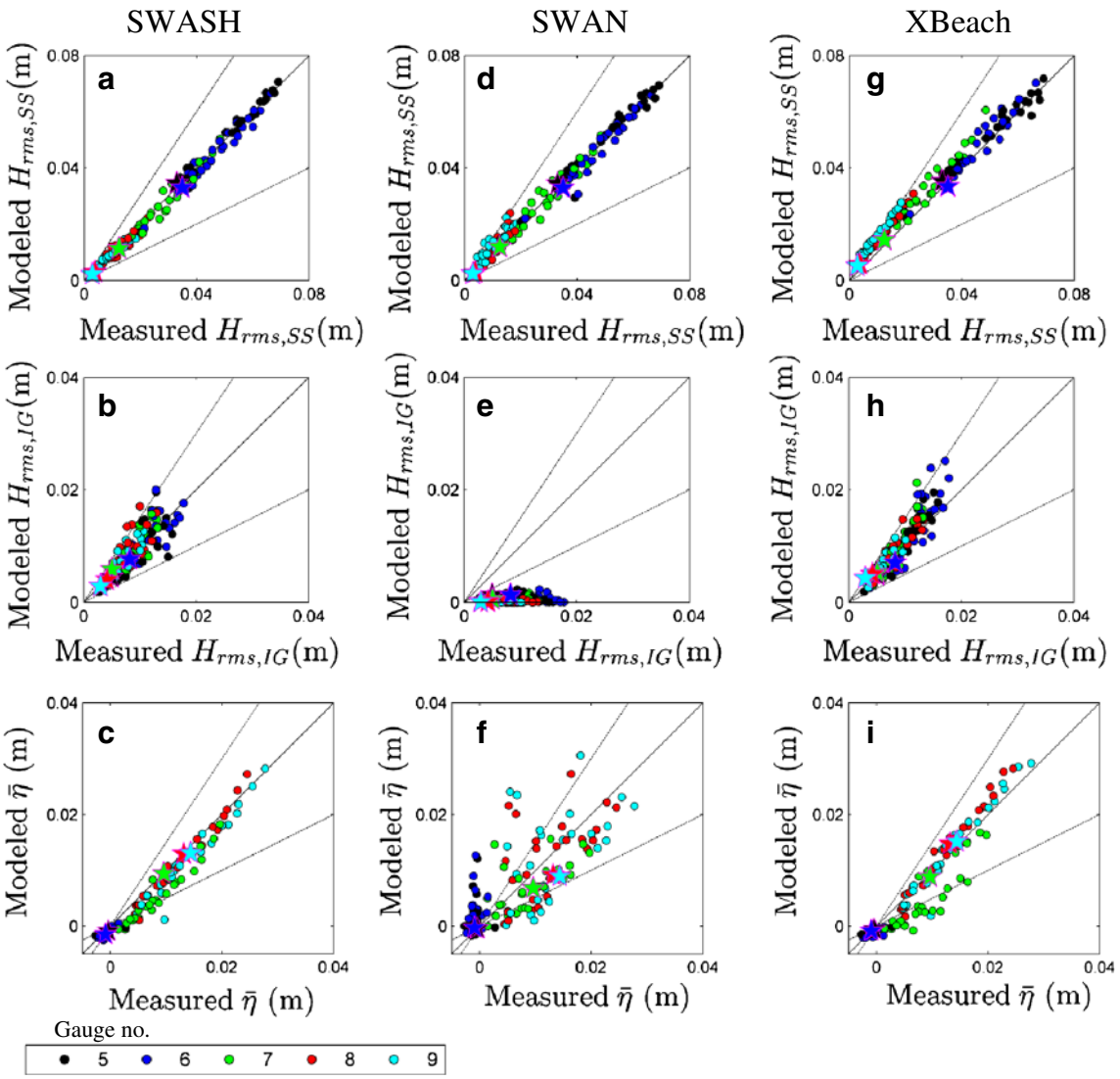

Fig. 5 **a**–**i** Comparison of the untuned model results with the observations of $H_{rms,SS}$ (*first row*), $H_{rms,IG}$ (*second row*), and $\overline{\eta}$ (*third row*). Measured values are given on the *x*-axis, and simulation results are given on the *y*-axis for SWASH (*first column*), SWAN (*second column*), and XBeach (*third column*). The 1:1 line (*solid black diagonal lines*) and 50 % error bounds (*dashed black lines*) are given for reference. *Point colors* correspond to gauge locations as given in the legend. *Stars* are used to highlight test no. 35

(1994) confirmed that $\partial\eta/\partial t$, is greater for plunging waves than spilling waves.

5.2 The role of the breaker parameter γ (XBeach and SWAN)

γ describes the maximum stable wave-height-to-water depth ratio, $H_{max}/(h+\overline{\eta})$; however, optimal γ values were found to differ in magnitude between SWAN (using BJ78) and XBeach (using R93), and in some cases, in the direction in which these parameters had to be tuned to generate optimal results. As seen in Fig. 8a (see Sect. 5.3 for a definition and discussion of F_{c0}), the measured values of $H_{rms,SS}/(h+\overline{\eta})$ vary widely across the reef profile; for example, for test no 35, values reach 1.6 at gauge 7 and 0.34 at gauge 8. As a consequence, a single maximum stable value can be difficult to establish. XBeach using the R93 wave-breaking formulation showed that lower γ values relative to the default (untuned) value were optimal; i.e., the average optimal γ for these test conditions was γ=0.33 versus γ=0.55 for the untuned case (Table 2). However, in contrast to XBeach, an average tuned value of $\gamma\sim0.70$ (untuned γ=0.73) was found for SWAN using BJ78, roughly equal to the untuned value. Importantly, γ in both R93 and BJ78 has a clear physical definition as $\gamma=H_{max}/(h+\overline{\eta})$; hence, optimal γ values should ideally not differ among different parametric wave-breaking dissipation formulations.

In SWAN, the dissipation of an individual wave, D_b is proportional to H^2_{max} (Eq. 7) and hence, through Eq. (8), is proportional to γ^2. This is not the case for XBeach, where D_b

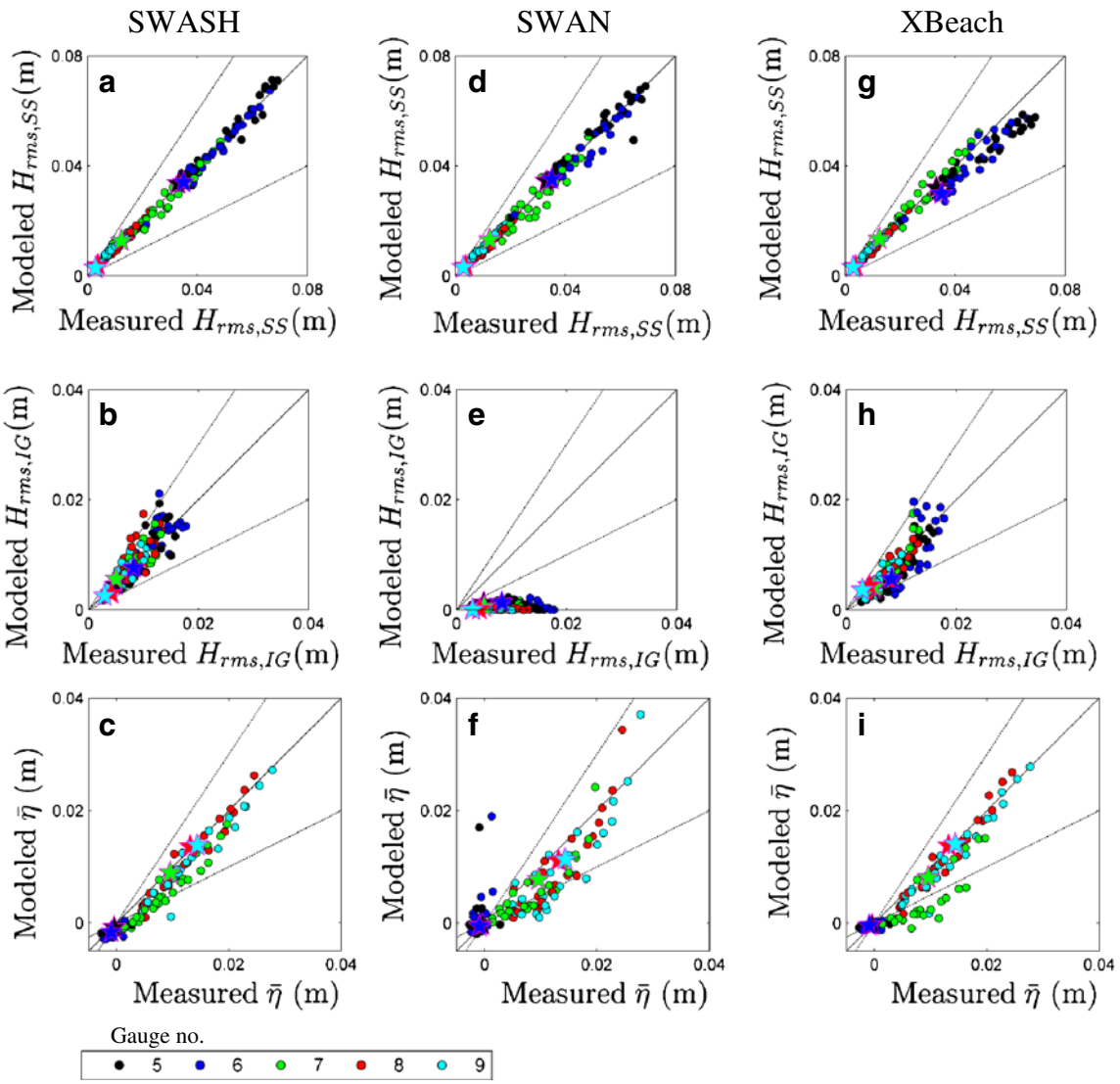

Fig. 6 **a**–**i** Comparison of the tuned model results with the observations of $H_{\mathrm{rms,SS}}$ (*first row*), $H_{\mathrm{rms,IG}}$ (*second row*), and $\bar{\eta}$ (*third row*). Measured values are given on the *x*-axis, and simulation results are given on the *y*-axis for SWASH (*first column*), SWAN (*second column*), and XBeach (*third column*). The 1:1 line (*solid black diagonal lines*) and 50 % error bounds (*dashed black lines*) are given for reference. *Point colors* correspond to gauge locations as given in the legend. *Stars* are used to highlight test no. 35

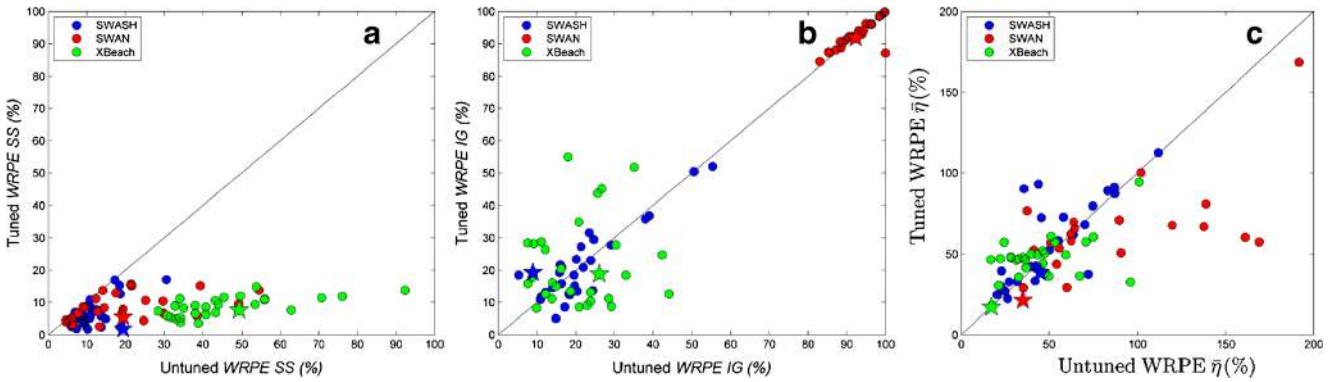

Fig. 7 Comparison of untuned (*x*-axis) and tuned (*y*-axis) **a** WRPE SS, **b** WRPE IG, and **c** WRPE $\bar{\eta}$ for the 29 test conditions for SWASH, SWAN, and XBeach. The 1:1 line is shown as the *solid black line*. Points above the 1:1 line are test conditions where the tuned model was less accurate than the untuned model; points below the 1:1 line are test conditions were the tuned model was more accurate than the untuned model. *Stars* are used to highlight test no. 35. Note the scale change for WRPE $\bar{\eta}$

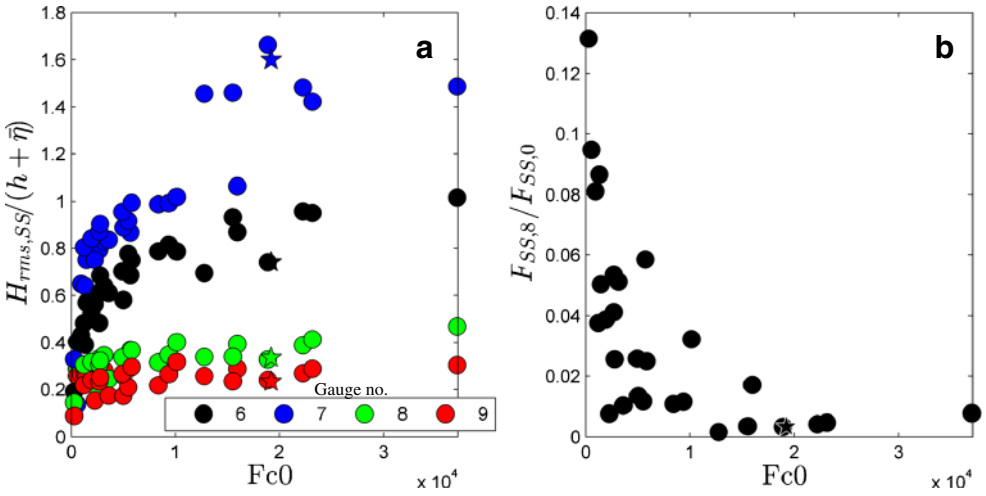

Fig. 8 Observed **a** $H_{rms,SS}/(h_r+\overline{\eta})$ and **b** dissipation (as expressed by $F_{SS,8}/F_{SS,0}$ where $F_{SS,8}$ and $F_{SS,0}$ are SS wave-energy flux on the reef flat (gauge 8) and deep water, respectively) as a function of the nonlinearity parameter, F_{c0} (see Sect. 5.3 for a definition and discussion of F_{c0}). *Stars* are used to highlight test no. 35

is proportional to $H^3_{rms,SS}/(h+\overline{\eta})$ and hence dependent on the local (not maximum) wave height per Eq. (10). These deviations in the formulations are the result of assumptions made in their derivation. Both BJ78 and R93 model formulations begin with

$$D_{tot} = D_b Q_b \tag{18}$$

$$D_b = \frac{1}{4}\rho g f B H^2 \frac{H}{\left(h+\overline{\eta}\right)} \tag{19}$$

where H is a representative local wave height. But, BJ78 then assumes that $H/(h+\overline{\eta})$ is roughly 1 and thus neglects the term; H is assumed to be H_{max} yielding Eq. (7). R93 assumes H to be equivalent to $H_{rms,SS}$ yielding Eq. (10). These seemingly minor differences in assumptions lead to divergence of the model predictions and are believed to be the main source of the difference in default and tuned γ values between SWAN and XBeach. H_{max} and Q_b formulations also differ between the two models. Notably, Q_b in R93 increases more rapidly than BJ78 as $H_{rms,SS}/(h+\overline{\eta})$ approaches γ. When increasing γ in either model, this results in shoreward shift of the break point and an increase in $H_{rms,SS}/(h+\overline{\eta})$ on the reef flat. In SWAN increasing γ also results in a γ^2 increase in D_b (assuming $\overline{\eta}$ remains constant). D_b can be thought of as the maximum dissipation rate (with Q_b=1 or 100 % wave-breaking $D_{tot}=D_b$). In SWAN, the maximum dissipation rate can be tuned by changing γ, whereas in XBeach, the maximum dissipation rate is independent of γ.

Test no. 35 provides an example of this difference in response to γ in SWAN and XBeach. Despite the smaller default value of γ in XBeach, with untuned γ values, XBeach predicts higher $H_{rms,SS}$ on the reef flat than SWAN and overpredicts SS wave heights over the reef flat (Fig. 3a). This overprediction of $H_{rms,SS}$ on the reef flat by XBeach was also observed in most test cases for the untuned simulations (Fig. 5g). To correct this overprediction, a much lower than default γ is needed (Table 2). Lowering γ results in a seaward shift of the break point and a broadening of the surf zone, thus underestimating the dissipation between gauges 6 and 7 but better matching $H_{rms,SS}$ across the reef flat (Fig. 3e). This underestimate in dissipation, which reduces the local radiation stress gradient, leads to a slight underestimate of $\overline{\eta}$ at gauge 7 (Fig. 3g). This can also be observed at gauge 7 for all test cases in Fig. 6i (green points below the 1:1 line). With the lower γ broadening the surf zone, dissipation continues between gauges 7 and 8 and the overestimate in $H_{rms,SS}$ and underestimate of $\overline{\eta}$ are corrected (Fig. 3e, g for test no 35 and Fig. 6g,i for all test cases).

5.3 Prediction of α and γ

Ideally, optimal α and γ values would be related to test conditions through a nondimensional parameter. For both laboratory and field data, obtained on plane and barred beach environments, Battjes and Stive (1985) (herein, after BS) found optimal γ values to be weakly dependent on offshore wave steepness (S_0), with γ given by

$$\gamma = 0.5 + 0.4[\tanh(33S_0)] \tag{20}$$

Nairn (1990) (herein, after NA) modified the empirical coefficient in BS, with γ given by

$$\gamma = 0.39 + 0.56[\tanh(33S_0)] \tag{21}$$

The NA formulation has subsequently been adopted for application to steep beaches by Baldock et al.

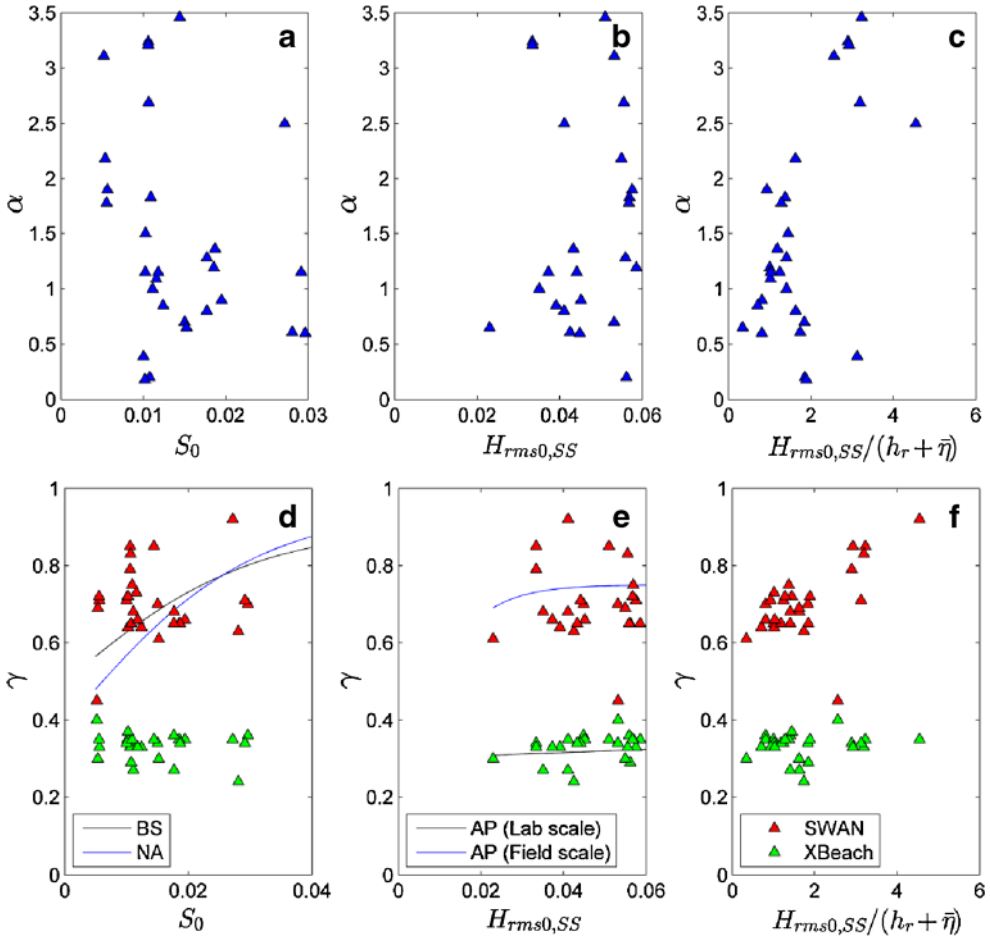

Fig. 9 **a**–**f** Ideally, optimal α and γ values could be related to a wave parameter, S_0, $H_{rms0,SS}$, and $H_{rms0,SS}$ ($h_r+\bar{\eta}$) have been proposed in the literature. Tuned α values for SWASH (*top row*) and tuned γ values for SWAN (*bottom row*; *red triangles*) and XBeach (*bottom row*; *green triangles*) are shown versus S_0, $H_{rms0,SS}$, and $H_{rms0,SS}/(h_r+\bar{\eta})$. The Battjes and Stive (1985) (BS) and the Nairn (1990) (NA) formulations are shown in **d**. The Apotsos et al. (2008) formulation for BJ78 (SWAN) is shown in **e** for laboratory scale and field scale (1:64 geometric scaling)

(1998) and Janssen and Battjes (2007). In a review of existing predictive γ formulations, Apotsos et al. (2008) instead found that optimal γ values for field observations, on mild-sloping beaches, were dependent on the offshore wave height ($H_{rms0,SS}$) and varied between wave-breaking formulations. Apotsos et al. (2008)

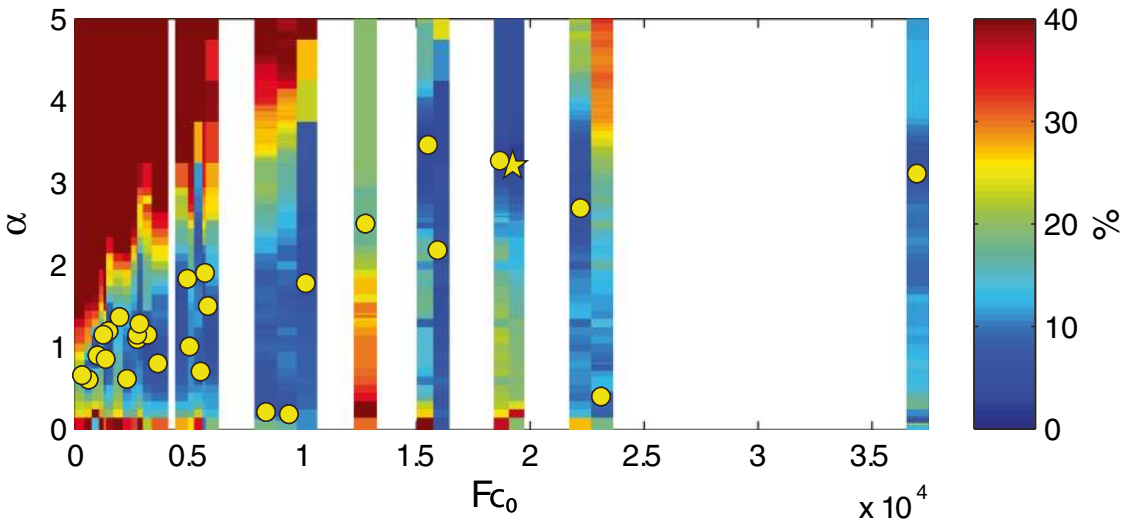

Fig. 10 Error in $H_{rms,SS}$ prediction (WRPE SS shown with *color bands*) for SWASH as a function of F_{c0} and α. *Individual color bands* give WRPE SS for a given test condition and α. *Yellow dots* give the optimum α for each test condition. The *yellow star* is the optimum α for test no. 35 ($H_{rms,SS}$=0.032 m; T_p=1.42; h_r=0.00 m)

(herein, after AP) developed a universal empirical relationship between γ and $H_{\mathrm{rms0,SS}}$, with the general form

$$\gamma = a + b\left[\tanh\left(cH_{\mathrm{rms0,SS}}\right)\right] \tag{22}$$

where a, b, and c are empirical coefficients fitted to observations. From an extensive review of field observations on sandy beaches, Apotsos et al. (2008) gives a=0.30, b=0.45, and c=0.90 m^{-1} for BJ78; R93 was not included in Apotsos et al. (2008). The dimensional dependence of AP would imply that contrary to conventional thinking, γ could differ between laboratory and field measurements. On fringing reef profiles, measured γ values at the break point have been related to the nondimensional relative water depth $(h_r+\overline{\eta})/H_{\mathrm{rms0,SS}}$ (see Yao et al. (2012) and references therein).

For the steep-slope Demirbilek et al. (2007) dataset, we do not find a clear dependence of the optimal α and γ values on S_0 (Fig. 9) in contrast to the findings of Battjes and Stive (1985) and Nairn (1990). There does however appear to be a general trend of increasing optimal α and γ values with $H_{\mathrm{rms0,SS}}/(h_r+\overline{\eta})$ (as well as with $H_{\mathrm{rms0,SS}}$ for XBeach) (Fig. 9).

The intensity of wave-breaking has been related to the nonlinearity parameter, F_{c0} (Nelson 1994; Gourlay 1994; Massel and Gourlay 2000; Sheremet et al. 2011).

$$F_{c0} = \frac{g^{1.25}H_{\mathrm{rms,0}}^{0.5}T_p^{2.5}}{\left(h_r+\overline{\eta}\right)^{1.75}} \tag{17}$$

where T_p is the peak wave period. Based on field and laboratory data from reef profiles with near horizontal reef flats,

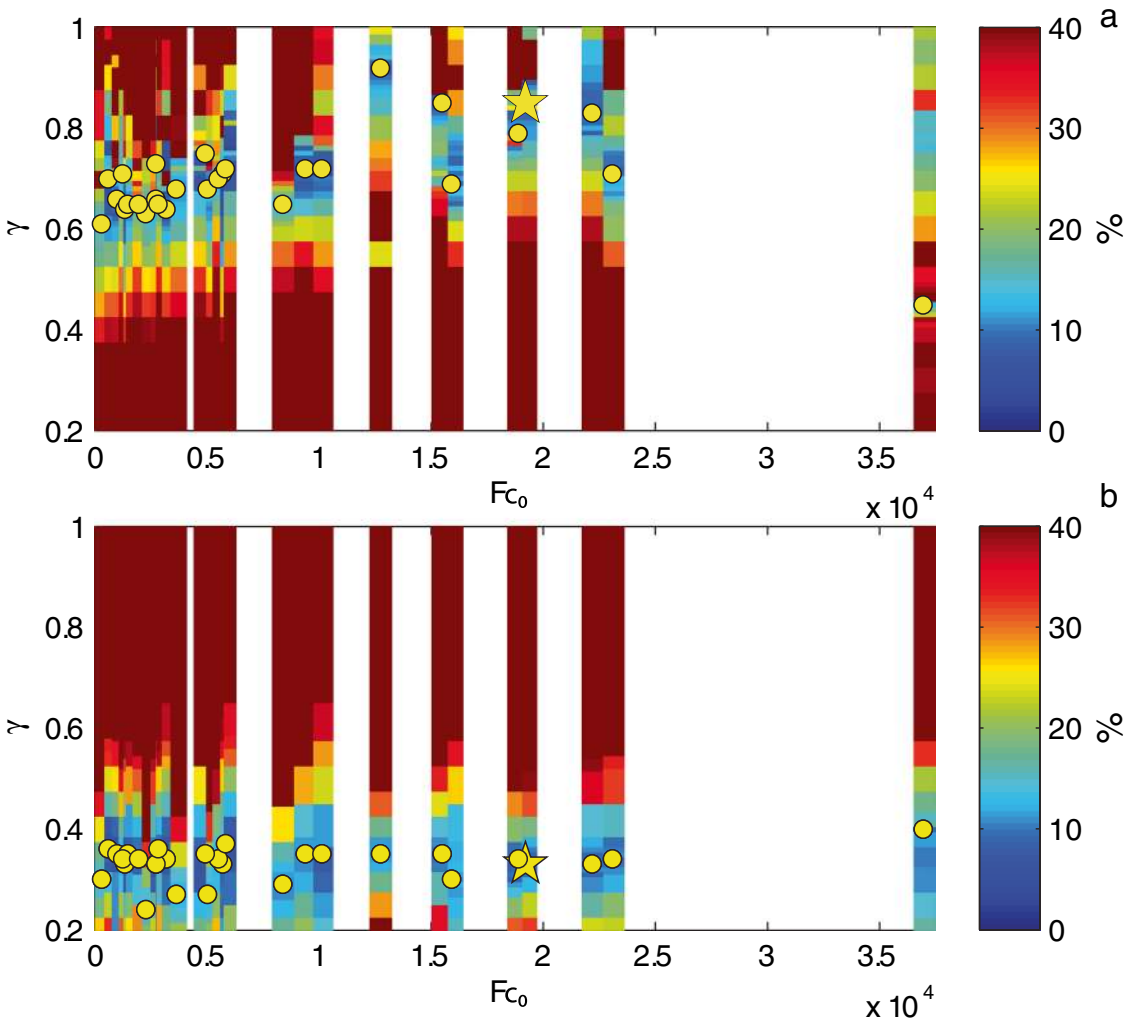

Fig. 11 Error in $H_{\mathrm{rms,SS}}$ prediction (WRPE SS shown with *color bands*) for SWAN (**a**) and Xbeach (**b**) as a function of F_{c0} and γ. *Individual color bands* give WRPE SS for a given test condition and γ. *Yellow dots* give the optimum α for each test condition. The *yellow star* is the optimum γ for test no. 35 ($H_{\mathrm{rms,SS}}$=0.032 m; T_p=1.42; h_r=0.00 m)

Nelson (1994) and Gourlay (1994) proposed that F_{c0} was suitable parameter for classifying relative wave shape and wave transformation. From observations, Fig. 8 shows that $H_{rms,SS}/(h+\overline{\eta})$ increases with F_{c0} for wave gauges on the fore reef (gauge 6) and reef flat (gauges 7, 8, and 9). Relative wave-breaking dissipation (as expressed by the energy-flux ratio $F_{SS,8}/F_{SS,0}$ where $F_{SS,8}$ and $F_{SS,0}$ are the SS wave-energy flux on the reef flat (gauge 8) and offshore, respectively) generally increased with increased F_{c0}.

Optimal α values for SWASH and γ values for SWAN generally increase (though with some notable exceptions) with F_{c0} (Figs. 10 and 11). In contrast, optimal γ values for XBeach remain relatively constant over the range of test conditions (Figs. 11). Figures 10 and 11 show the WRPE SS error metric as a function of each model's key wave-breaking parameter and F_{c0}, with optimal values of α and γ shown with points. For F_{c0} $<1\times10^4$ SWASH had high WRPE SS errors for large values of α. As F_{c0} increased in the 3×10^2 to 1×10^4 range, the values of α which predicted high WRPE SS errors increased. For $F_{c0}>$ 1×10^4 SWASH generally showed less sensitivity to α values. With the exception of three test conditions, optimal α values for SWASH increased with F_{c0}. Test nos. 30, 31, and most notably 38 give lower than default optimal α (0.20, 0.18, and 0.39, respectively; Table 2). In these three scenarios, the default α resulted in an overprediction of $H_{rms,SS}$ at gauges on the reef flat and lower α values were required to reduce $H_{rms,SS}$ on the reef flat. It is however unclear why the overprediction with the untuned α exists for these three scenarios, as the scenarios fit the general trend of increasing $H_{rms,SS}/(h+\overline{\eta})$ with F_{c0} (Fig. 8a) and increased dissipation with F_{c0} (Fig. 8b). Overall, as depicted in Fig. 5, we must emphasize that the SWASH results with the untuned α=0.6 still agree well with measurements, but further improvement was possible by this tuning of α (Table 2; Fig. 7).

Over the range of F_{c0} values, for γ from 0.2 to 1, SWAN and XBeach showed contrasting regions of high WRPE SS (Fig. 11). SWAN predictions gave high WRPE SS for γ $<\sim0.5$; however, XBeach predictions showed high WRPE SS for $\gamma>\sim0.5$ (Fig. 11). Also, SWAN predictions showed a general increase in optimal γ values with F_{c0}, whereas this trend is not present for XBeach predictions. The differing optimal γ values and response to F_{c0} for SWAN and XBeach are believed to be due to differences in the breaking formulation discussed in Sect. 5.2.

6 Conclusions

In this test of three commonly used wave models (SWASH, SWAN, and XBeach), all were found to be capable of predicting SS wave height variations across a steep fringing reef profile with reasonable accuracy (Fig. 5 a, d, g and Fig. 7a). Nevertheless, with tuning of the wave-breaking parameters (α in SWASH and γ in both SWAN and XBeach), the accuracy of predictions could be further increased substantially (Table 2; Fig. 6 a, d, g; Fig. 7a). SWASH and XBeach also predicted IG wave height (Fig. 5 b, h; Fig. 6 b, h; Fig. 7b) and spectral transformation into lower frequencies (Fig. 4), albeit with higher error than for the SS waves. Although SWAN was capable of accurately modeling the SS wave heights, in its current form, it was not able to accurately model the observed spectral transformation into lower frequencies, as evident in the underprediction of IG waves across the reef flat (Figs. 3, 4, 5, 6, and 7). Recently, Sheremet et al. (2011) showed that it is possible to accurately model spectral transformation (including IG waves) using a nonlinear spectral wave model with direct nonlinear triad interaction and frequency dependent wave-breaking. Spectral transformation in SWAN may thus be improved by adopting some of the formulations found in Sheremet et al. (2011). The skill of either SWAN or XBeach could potentially be improved by using an alternative wave-breaking dissipation formula or implementing a spatially variable γ formulation (e.g., van der Westhuysen (2010)). Furthermore, comparative testing needs to be conducted to look at other reef geometries and test cases that include larger more realistic bottom roughness. The accuracy of predictions of other metrics (e.g., skewness and asymmetry of velocity and acceleration), not just wave height, that are also important for predicting wave-driven currents and sediment transport should also be further investigated. In general, the capabilities of these nonreef/steep-slope-specific beach models show promise when applied to these environments.

Acknowledgments We are grateful to Ap Van Dongeren and Dano Roelvink for the helpful discussion of the XBeach model. This project forms part of a Ph.D. study by M. Buckley at The University of Western Australia and is supported by an International Postgraduate Research Scholarships. R. Lowe was supported by an Australian Research Council Future Fellowship.

References

Apotsos A, Raubenheimer B, Elgar S, Guza RT, Smith JA (2007) Effects of wave rollers and bottom stress on wave setup. J Geophys Res 112 (C2). doi:10.1029/2006jc003549

Apotsos A, Raubenheimer B, Elgar S, Guza RT (2008) Testing and calibrating parametric wave transformation models on natural beaches. Coast Eng 55(3):224–235. doi:10.1016/j.coastaleng.2007.10.002

Baldock T, Holmes P, Bunker S, Van Weert P (1998) Cross-shore hydrodynamics within an unsaturated surf zone. Coast Eng 34(3–4):173–196

Battjes JA, Janssen JPFM (1978) Energy loss and set-up due to breaking of random waves. Proc 16th Int Conf Coast Eng, ASCE:569-587

Battjes JA, Stive MJF (1985) Calibration and verification of a dissipation model for random breaking waves. J Geophys Res Oceans 90(C5): 9159–9167. doi:10.1029/JC090iC05p09159

Booij N, Ris RC, Holthuijsen LH (1999) A third-generation wave model for coastal regions 1. Model description and validation. J Geophys Res C Oceans 104(C4):7649–7666

Cavaleri L, Alves JHGM, Ardhuin F, Babanin A, Banner M, Belibassakis K, Benoit M, Donelan M, Groeneweg J, Herbers THC, Hwang P, Janssen PAEM, Janssen T, Lavrenov IV, Magne R, Monbaliu J, Onorato M, Polnikov V, Resio D, Rogers WE, Sheremet A, McKee Smith J, Tolman HL, van Vledder G, Wolf J, Young I (2007) Wave modelling—the state of the art. Prog Oceanogr 75(4):603–674. doi:10.1016/j.pocean.2007.05.005

Cienfuegos R, Barthélemy E, Bonneton P (2010) Wave-breaking model for Boussinesq-type equations including roller effects in the mass conservation equation. J Waterw Port Coast Ocean Eng 136(1):10–26. doi:10.1061/(asce)ww.1943-5460.0000022

Demirbilek Z, Nwogu OG (2007) Boussinesq Modeling of Wave Propagation and Runup over Fringing Coral Reefs, Model Evaluation Report. Data Report ERDC/CHL TR-07-12, Coastal and Hydraulics Laboratory

Demirbilek Z, Nwogu OG, Ward DL (2007) Laboratory Study of Wind Effect on Runup over Fringing Reefs, Report 1: Data Report. ERDC/CHL TR-07-4, Coastal and Hydraulics Laboratory

Feddersen F, Gallagher EL, Guza RT, Elgar S (2003) The drag coefficient, bottom roughness, and wave-breaking in the nearshore. Coast Eng 48(3):189–195. doi:10.1016/s0378-3839(03)00026-7

Filipot J-F, Cheung KF (2012) Spectral wave modeling in fringing reef environments. Coast Eng 67:67–79. doi:10.1016/j.coastaleng.2012.04.005

Gourlay MR (1994) Wave transformation on a coral reef. Coast Eng 23(1–2):17–42. doi:10.1016/0378-3839(94)90013-2

Gourlay MR, Colleter G (2005) Wave-generated flow on coral reefs—an analysis for two-dimensional horizontal reef-tops with steep faces. Coast Eng 52(4):353–387. doi:10.1016/j.coastaleng.2004.11.007

Hasselmann DE, Dunckel M, Ewing JA (1980) Directional wave spectra observed during JONSWAP 1973. J Phys Oceanogr 10(8):1264–1280. doi:10.1175/1520-0485(1980)010<1264:dwsodj>2.0.co;2

Hearn CJ (1999) Wave-breaking hydrodynamics within coral reef systems and the effect of changing relative sea level. J Geophys Res 104(C12):30007–30019. doi:10.1029/1999jc900262

Hoeke R, Storlazzi C, Ridd P (2011) Hydrodynamics of a bathymetrically complex fringing coral reef embayment: Wave climate, in situ observations, and wave prediction. J Geophys Res-Oceans 116. doi:10.1029/2010jc006170

Janssen TT, Battjes JA (2007) A note on wave energy dissipation over steep beaches. Coast Eng 54(9):711–716. doi:10.1016/j.coastaleng.2007.05.006

Lowe RJ, Falter JL, Bandet MD, Pawlak G, Atkinson MJ, Monismith SG, Koseff JR (2005) Spectral wave dissipation over a barrier reef. J Geophys Res 110(C4), C04001. doi:10.1029/2004jc002711

Lowe RJ, Falter JL, Monismith SG, Atkinson MJ (2009) A numerical study of circulation in a coastal reef-lagoon system. J Geophys Res 114(C6), C06022. doi:10.1029/2008jc005081

Madsen PA, Sørensen OR, Schäffer HA (1997) Surf zone dynamics simulated by a Boussinesq type model. Part I. Model description and cross-shore motion of regular waves. Coast Eng 32(4):255–287. doi:10.1016/s0378-3839(97)00028-8

Mansard EPD, Funke ER (1980) Measurement of incident and reflected spectra using a least squares method. 17th International Conference on Coastal Engineering, Sydney, Australia:pp. 95–96

Massel SR, Gourlay MR (2000) On the modelling of wave breaking and set-up on coral reefs. Coast Eng 39(1):1–27. doi:10.1016/s0378-3839(99)00052-6

Murphy AH, Epstein ES (1989) Skill scores and correlation coefficients in model verification. Mon Weather Rev 117(3):572–582. doi:10.1175/1520-0493(1989)117<0572:ssacci>2.0.co;2

Nairn RB (1990) Prediction of cross-shore sediment transport and beach profile evolution. Imperial College, London

Nelson RC (1994) Depth limited design wave heights in very flat regions. Coast Eng 23(1–2):43–59. doi:10.1016/0378-3839(94)90014-0

Pomeroy A, Lowe R, Symonds G, Van Dongeren A, Moore C (2012) The dynamics of infragravity wave transformation over a fringing reef. J Geophys Res-Oceans 117. doi:10.1029/2012jc008310

Reniers AJHM, Battjes JA (1997) A laboratory study of longshore currents over barred and non-barred beaches. Coast Eng 30(1–2):1–21. doi:10.1016/S0378-3839(96)00033-6

Roelvink JA (1993) Dissipation in random wave groups incident on a beach. Coast Eng 19(1–2):127–150. doi:10.1016/0378-3839(93)90021-y

Roelvink D, Reniers A, van Dongeren A, van Thiel de Vries J, McCall R, Lescinski J (2009) Modelling storm impacts on beaches, dunes and barrier islands. Coast Eng 56(11–12):1133–1152. doi:10.1016/j.coastaleng.2009.08.006

Ruessink BG, Walstra DJR, Southgate HN (2003) Calibration and verification of a parametric wave model on barred beaches. Coast Eng 48(3):139–149. doi:10.1016/S0378-3839(03)00023-1

Schäffer HA, Madsen PA, Deigaard R (1993) A Boussinesq model for waves breaking in shallow water. Coast Eng 20(3–4):185–202. doi:10.1016/0378-3839(93)90001-o

Sheremet A, Kaihatu JM, Su SF, Smith ER, Smith JM (2011) Modeling of nonlinear wave propagation over fringing reefs. Coast Eng 58(12):1125–1137. doi:10.1016/j.coastaleng.2011.06.007

Smit P, Zijlema M, Stelling G (2013) Depth-induced wave breaking in a non-hydrostatic, near-shore wave model. Coast Eng 76:1–16. doi:10.1016/j.coastaleng.2013.01.008

Storlazzi CD, Elias E, Field ME, Presto MK (2011) Numerical modeling of the impact of sea-level rise on fringing coral reef hydrodynamics and sediment transport. Coral Reefs 30:83–96. doi:10.1007/s00338-011-0723-9

Svendsen IA (1984) Mass flux and undertow in a surf zone. Coast Eng 8(4):347–365. doi:10.1016/0378-3839(84)90030-9

Symonds G, Black KP, Young IR (1995) Wave-driven flow over shallow reefs. J Geophys Res 100(C2):2639–2648. doi:10.1029/94jc02736

Ting FCK, Kirby JT (1994) Observation of undertow and turbulence in a laboratory surf zone. Coast Eng 24(1–2):51–80. doi:10.1016/0378-3839(94)90026-4

Torres-Freyermuth A, Marino-Tapia I, Coronado C, Salles P, Medellin G, Pedrozo-Acuna A, Silva R, Candela J, Iglesias-Prieto R (2012) Wave-induced extreme water levels in the Puerto Morelos fringing reef lagoon. Nat Hazard Earth Syst 12(12):3765–3773. doi:10.5194/nhess-12-3765-2012

van der Westhuysen AJ (2010) Modeling of depth-induced wave breaking under finite depth wave growth conditions. J Geophys Res Oceans 115(C1), C01008. doi:10.1029/2009jc005433

Van Dongeren A, Lowe R, Pomeroy A, Trang DM, Roelvink D, Symonds G, Ranasinghe R (2013) Numerical modeling of low-frequency wave dynamics over a fringing coral reef. Coast Eng 73:178–190. doi:10.1016/j.coastaleng.2012.11.004

Yao Y, Huang Z, Monismith SG, Lo EYM (2012) Characteristics of Monochromatic Waves Breaking over Fringing Reefs. J Coast Res:94-104. doi:10.2112/jcoastres-d-12-00021.1

Zijlema M (2012) Modelling wave transformation across a fringing reef using SWASH. Coast Eng Proc 1(33) (currents.26). doi:10.9753/icce.v33.currents.26

Zijlema M, Stelling GS (2008) Efficient computation of surf zone waves using the nonlinear shallow water equations with non-hydrostatic pressure. Coast Eng 55(10):780–790. doi:10.1016/j.coastaleng.2008.02.020

Zijlema M, Stelling G, Smit P (2011) SWASH: an operational public domain code for simulating wave fields and rapidly varied flows in coastal waters. Coast Eng 58(10):992–1012. doi:10.1016/j.coastaleng.2011.05.015